



## SOME NUMERICAL ASPECTS OF A LINEAR STATIC ISOGEOMETRIC ANALYSIS OF AN ARBITRARILY CURVED PLANE BERNOULLI-EULER BEAM

Aleksandar Borković, [aleksandar.borkovic@aggf.unibl.org](mailto:aleksandar.borkovic@aggf.unibl.org), University of Banja Luka, Faculty of Architecture, Civil Engineering and Geodesy

Gligor Radenković, [radenkovic@grf.bg.ac.rs](mailto:radenkovic@grf.bg.ac.rs), University of Belgrade, Faculty of Civil Engineering

Snježana Milovanović, [snjezana\\_milovanovic@yahoo.com](mailto:snjezana_milovanovic@yahoo.com), University of Banja Luka, Faculty of Architecture, Civil Engineering and Geodesy

Dijana Majstorović, [dijana.majstorovic@aggf.unibl.org](mailto:dijana.majstorovic@aggf.unibl.org), University of Banja Luka, Faculty of Architecture, Civil Engineering and Geodesy

### **Abstract:**

Linear static analysis of arbitrarily curved beams is considered. Metric of a Bernoulli-Euler beam is rigorously defined and the weak form of the corresponding boundary-value problem is solved using isogeometric approach. Driving force behind present research is detail numerical analysis of recently developed model of an arbitrarily curved beam. This is obtained via in-depth analysis of convergence properties, as well as by comparison with other numerical models. Excellent agreement of results is obtained and improved accuracy of the model with the highest continuity is proved to be valid for most cases.

*Keywords:* arbitrarily curved beam; isogeometric analysis; structural modeling

## НЕКИ НУМЕРИЧКИ АСПЕКТИ ЛИНЕАРНЕ СТАТИЧКЕ ИЗОГЕОМЕТРИЈСКЕ АНАЛИЗЕ ПРОИЗВОЉНО КРИВЕ БЕРНУЛИ-ОЈЛЕРОВЕ ГРЕДЕ

### **Резиме:**

У раду је размотрена линеарна статичка анализа произвољно кривих греда. Метрика Бернули-Ојлерове греде је строго дефинисана, након чега је, примјеном изогеометријског приступа, ријешена слаба форма одговарајућег граничног проблема. Основни мотив за провођење датог истраживања слиједи из уочене потребе за детаљном нумеричком анализом недавно развијеног модела произвољно криве греде. Ова анализа је извршена пажљивим разматрањем особина конвергенције посматраног модела, као и кроз поређење са другим нумеричким моделима. Добијено је одлично поклапање резултата при чему је потврђена чињеница да модели са највишим континуитетом често имају побољшану тачност.

*Кључне ријечи:* произвољно крива греда, изогеометријска анализа, моделирање конструкција

## 1. INTRODUCTION

Curved beams are increasing in popularity as structural elements. They have significant aesthetical value and great versatility when it comes to free-form modeling. Introduction of contemporary materials with improved mechanical properties enabled development of structural forms not previously imaginable. Consequently, there is an increase in necessity for development of efficient computational models for these structures. Besides standard isoparametric finite element (FE) method, during past decade we have witnessed an extensive growth of so-called isogeometric analysis (IGA), which is ideally suited for analysis of curved structures, [1]. The logic of IGA approach is reverse in comparison with isoparametric concept, [2]. Namely, isogeometric approach defines the structural geometry primarily and, most often, exactly. This is enabled due to versatility of basis functions, non-uniform rational basis spline (NURBS) being the most prominent one. Afterwards, the same adopted basis functions are utilized for description of kinematics. IGA is developed as a tool which could bridge gap between design and analysis, which it partially succeeded but more research is in front of us. Some of the actual topics are trimmed geometries, optimal quadrature rules etc. [3].

Analysis of curved beams in the frame of IGA is frequent, especially regarding Timoshenko beam model, see for example [4]. However, especially attractive feature of Bernoulli-Euler (BE) beam model is potential to introduce rotation-free models, since, for this theory, the rotation of a cross section is a function of translations of beam axis.

Aim of this paper is to investigate some numerical aspects of rotation-free IGA of an arbitrarily curved BE beam following recent findings given in [5], [6] and [7]. Detail analysis of influence of NURBS order and continuity on convergence properties is performed.

Paper is organized in five sections. After this brief introduction, some basic concepts regarding NURBS-based IGA modeling is presented. Numerical model is given in third section where abbreviated derivation of beam metric is given and followed with finite element formulation. Numerical analysis of two examples is performed in fourth section after which brief conclusions are drawn.

## 2. NURBS-BASED ISOGEOMETRIC MODELING

Brief consideration of NURBS functions is given. For more detailed discussion on this topic, refer to [8] and [9].

### 2.1. Non-uniform B-spline

B-splines are piecewise polynomial curves defined as:

$$\mathbf{r}(\xi) = \sum_{i=1}^N B_{i,p}(\xi) \mathbf{P}_i, \quad (1)$$

where  $\mathbf{P}_i \in \mathbb{R}^d$  are control points and  $B_{i,p}(\xi)$  are the  $p^{\text{th}}$  order B-spline basis functions. Line segments that connect consecutive control points form the so-called control polygon. The B-spline basis functions are defined by a knot vector  $\xi = \{\xi_1, \xi_2, \dots, \xi_{N+p+1}\}$ , a non-decreasing sequence of real numbers, called knots. The same knot value may appear in a knot vector more than once and it is called a multiple knot. The knots partition the parameter space into knot spans, which also have representations in a physical space and parent domain, Fig. 1. Each non-zero knot span represents an isogeometric finite element.

If the first and the last knot have multiplicity  $p + 1$ , the knot vector is said to be open. In this research, we employ only open knot vectors. Depending on whether the knot spans are equal or not, knot vectors may be uniform or non-uniform.

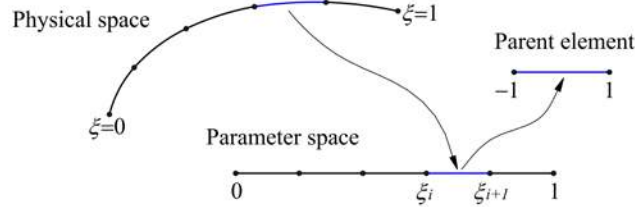


Figure 1. Physical space, parameter space and parent element

With a given knot vector, the B-spline basis functions are defined by the Cox-de Boor recursion formula, starting with piecewise constants ( $p = 0$ ):

$$B_{i,0}(\xi) = \begin{cases} 1 & \text{if } \xi_i \leq \xi < \xi_{i+1}, \\ 0 & \text{otherwise} \end{cases}, \quad (2)$$

$$B_{i,p}(\xi) = \frac{\xi - \xi_i}{\xi_{i+p} - \xi_i} B_{i,p-1}(\xi) + \frac{\xi_{i+p+1} - \xi}{\xi_{i+p+1} - \xi_{i+1}} B_{i+1,p-1}(\xi).$$

Some of the important properties of basis functions are that they constitute a partition of unity and they are non-negative for any value of parameter  $\xi$ . In each knot span, at most  $p + 1$  basis functions are non-zero, which is referred as a local support property. B-spline basis function is  $C^{p-m}$  continuous at knots of multiplicity  $m$ . Basis functions formed from open knot vectors are interpolatory at the ends of parametric interval and also at knots whose multiplicity is equal to a polynomial order. The properties of B-spline curves follow directly from those of their basis functions.

Non-Uniform Rational B-spline (NURBS) is a generalization of B-spline functions that allows us to exactly represent a wide range of objects that cannot be represented with simple polynomials, such as conic sections. Rational B-spline is obtained by a projective transformation of higher dimensional B-spline and can be defined as:

$$\mathbf{r}(\xi) = \frac{\sum_{i=1}^N B_{i,p}(\xi) w_i \mathbf{P}_i}{\sum_{j=1}^N B_{j,p}(\xi) w_j} = \sum_{i=1}^N R_{i,p}(\xi) \mathbf{P}_i, \quad (3)$$

where  $w_i$  are the weights and  $R_{i,p}$  are the rational basis functions. Rational basis functions share the same main properties with the B-spline basis. If all weights are set to be equal, the NURBS curve becomes B-Spline.

An example of a cubic NURBS curve and corresponding rational basis is presented in Fig. 2. The curve is interpolatory and tangent to the control polygon at first and last control point and also at the sixth control point, since the multiplicity of the knot  $\xi = 3$  is  $m = 3$ . Increasing the weight  $w_5$  affects the curve shape only in the interval (1,3), where associated basis function is non-zero and a curve is pushed toward the control point. At the location of repeated knot, the curve is  $C^0$  continuous.

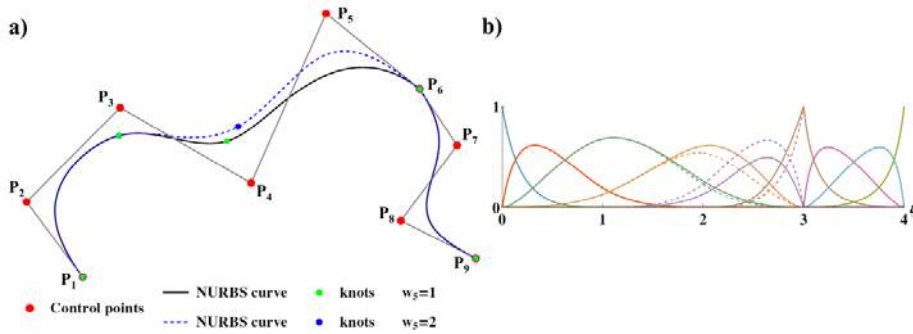


Figure 2. (a) NURBS curve with modification of  $w_5$  (b) Cubic rational bases defined with knot vector  $\xi = \{0, 0, 0, 0, 1, 2, 3, 3, 3, 4, 4, 4, 4\}$  and weights  $\mathbf{w} = \{1, 2, 3, 2, 1, 1, 3, 3, 1\}$  (solid line). For  $w_5 = 2$ , corresponding rational basis are changed (dashed line).

## 2.2. Mesh refinement

The knot insertion ( $h$ -refinement) consist in adding new knots in a knot vector while the geometry and parameterization of the original curve stay intact. Inserting new knot values result in splitting the existing elements into smaller ones. If inserted knot was already present in a knot vector, the continuity of basis functions will be reduced and no new elements will be created. In this research,  $h$ -refinement implies increasing the number of elements while polynomial order and continuity remain fixed.

The  $p$ -refinement (i.e. order elevation) strategy involves increasing the polynomial order of basis functions without changing the curve geometrically or parametrically. During the order elevation, continuity of basis functions is preserved by increasing the multiplicity of knots. The number of elements remains unchanged since no new knot values are added.

The fact that the knot insertion and order elevation processes do not commute, allows us to elevate an order on a coarsest mesh and than perform knot insertion. As a result, the continuity of basis functions can be increased. This is referred to as  $k$ -refinement strategy. Pictorial representation of  $p$ - and  $k$ -refinement procedures, applied on a patch with three elements, is displayed in Fig. 3.

## 3. THEORETICAL CONSIDERATIONS

Present derivations are based on the classic BE assumption: cross sections are absolutely rigid and orthogonal to the deformed beam axis. Consequence of this assumption is the degeneration of a 3D beam model into its 1D counterpart, Fig 4. The convective frame of reference  $(\xi, \eta, \zeta)$  is utilized with appropriate base vectors  $(\mathbf{g}_1, \mathbf{g}_2, \mathbf{g}_3)$ . At the centroid, curvilinear coordinate axis  $\xi$  correspond to the beam axis while  $\eta$  and  $\zeta$  are aligned with the principal axes of the second moment of area of a cross section, Fig 4. Due to introduced assumption,  $\xi$  is the only independent variable for the analysis of plane BE beams. Notice that base vectors  $(\mathbf{g}_2, \mathbf{g}_3)$  remain unit for all configurations. Present derivations are compact version of the ones given in [7] and [5].

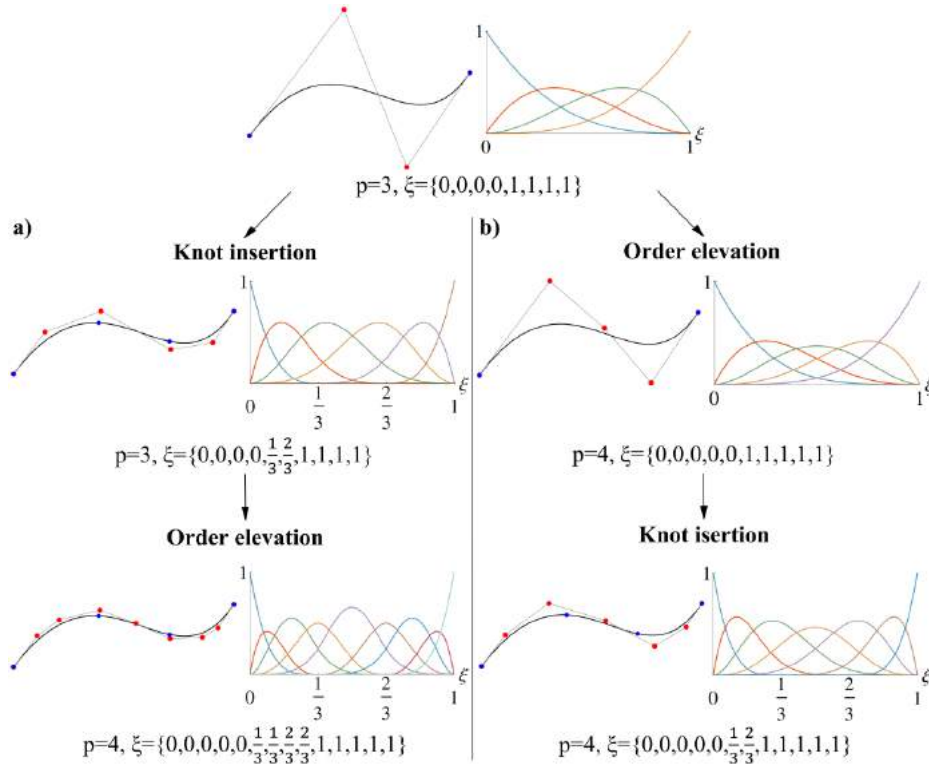


Figure 3. Higher-order meshes for: (a)  $p$ -refinement (b)  $k$ -refinement

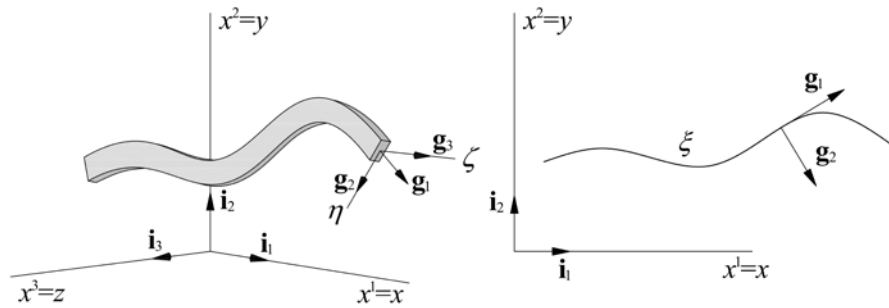


Figure 4. Degeneration of 3D beam into 1D; Coordinate systems and base vectors

### 3.1. REFERENCE CONFIGURATION OF BEAM AXIS

Position vector of the beam axis is  $\mathbf{r} = \mathbf{r}(\xi)$  while its Cartesian coordinates are  $x^\alpha = x^\alpha(\xi)$ ,  $\alpha = 1, 2$ . Hence, the position vector of beam axis and its base vector are:

$$\mathbf{r} = x^\alpha \mathbf{i}_\alpha, \quad \mathbf{g}_1 = \mathbf{r}_{,1} = \frac{d\mathbf{r}}{d\xi} = x_{,1}^\alpha \mathbf{i}_\alpha, \quad (4)$$

where  $()_{,k}$  designates differentiation with respect to the  $k^{\text{th}}$  coordinate of the system  $(\xi, \eta)$ .  $\mathbf{i}^\alpha$  are the unit base vectors of the Cartesian coordinate system, Fig. 4.

Classic relation of convective and arc-length coordinates is:

$$ds^2 = (x_{,1}^\alpha)^2 d\xi^2 = g_{11} d\xi^2 \Rightarrow ds = \sqrt{g_{11}} d\xi, \quad (5)$$

where  $g_{11}$  is the component of the metric tensor of a beam axis:

$$g_{\alpha\beta} = \begin{bmatrix} g_{11} & 0 \\ 0 & 1 \end{bmatrix} \Rightarrow \det g_{\alpha\beta} = g_{11}. \quad (6)$$

Base vector  $\mathbf{g}_1$  is collinear with tangent and its first derivative with respect to  $\xi$  is:

$$\mathbf{g}_1 = \sqrt{g_{11}} \mathbf{t}, \quad \mathbf{g}_{1,1} = \Gamma_{11}^1 \mathbf{g}_1 + \bar{K} \mathbf{g}_2, \quad \bar{K} = g_{11} K, \quad \Gamma_{11}^1 = x_{,1}^\alpha x_{\alpha,11} g^{11}. \quad (7)$$

where  $K$  is the modulus of curvature vector with respect to the Frenet-Serret frame of reference, while  $\bar{K}$  is its counterpart but with respect to the convective frame of reference.  $\Gamma_{11}^1$  is the Christoffel symbol of the second kind while the determinant of the contravariant metric tensor of the beam axis is  $g_{11} = g^{11}$ . The base vector of  $\eta$  coordinate follows from (7):

$$\mathbf{g}_2 = x_{,2}^\alpha \mathbf{i}_\alpha, \quad \mathbf{g}_2 = \frac{1}{\bar{K}} (\mathbf{g}_{1,1} - \Gamma_{11}^1 \mathbf{g}_1) \Rightarrow x_{,2}^\alpha = \frac{1}{\bar{K}} (x_{,11}^\alpha - \Gamma_{11}^1 x_{,1}^\alpha). \quad (8)$$

### 3.2. METRIC OF DEFORMED BEAM AXIS AND REFERENCE STRAINS

The position vector of the beam axis in the deformed configuration is:

$$\mathbf{r}^*(\xi) = \mathbf{r}(\xi) + \mathbf{u}(\xi), \quad (9)$$

where  $\mathbf{u}(\xi)$  is its displacement vector while tangential base vector of the beam axis is:

$$\mathbf{g}_1^* = \mathbf{r}_{,1}^* = (x_{,1}^\alpha + u_{,1}^\alpha) \mathbf{i}_\alpha = x_{,1}^{\alpha*} \mathbf{i}_\alpha. \quad (10)$$

Notice the determinant of the metric tensor of the deformed beam axis:

$$g_{11}^* = x_{,1}^{\alpha*} x_{\alpha,1}^*. \quad (11)$$

Additionally, normal base vector of the deformed beam axis is:

$$\mathbf{g}_2^* = \mathbf{g}_2 + \mathbf{u}_{,2}, \quad |\mathbf{g}_2^*| = |\mathbf{g}_2| = 1. \quad (12)$$

where:

$$\mathbf{u}_{,2} = -(\mathbf{g}_2 \cdot \mathbf{u}_{,1}) \mathbf{g}_1^1 = -\frac{1}{g_{11}} (\mathbf{g}_2 \cdot \mathbf{u}_{,1}) \mathbf{g}_1, \quad u_{,2} = -B_\alpha^\beta u_{\beta,1}, \quad B_\alpha^\beta = \frac{1}{g} x_{,2}^\beta x_{\alpha,1}. \quad (13)$$

The modulus of curvature of the deformed beam axis follows, analogous to (7):

$$\mathbf{g}_{1,1}^* = \Gamma_{11}^{*1} \mathbf{g}_1^* + \bar{K}^* \mathbf{g}_2^* \Rightarrow \bar{K}^* = \mathbf{g}_{1,1}^* \cdot \mathbf{g}_2^*. \quad (14)$$

Only Lagrange component of strain for linear BE theory is:

$$\varepsilon_{11} = \frac{1}{2} (g_{11}^* - g_{11}) \Rightarrow \varepsilon_{11} = x_{,1}^\alpha u_{\alpha,1}. \quad (15)$$

Additionally, the flexural strain of the beam axis is introduced as:

$$\kappa = \bar{K}^* - \bar{K} = \mathbf{g}_{1,1}^* \cdot \mathbf{g}_2^* - \mathbf{g}_{1,1} \cdot \mathbf{g}_2. \quad (16)$$

Using the BE conditions, as well as neglecting higher order terms of displacement gradients, we can obtain following relation:

$$\kappa = \mathbf{u}_{,11} \cdot \mathbf{g}_2 - \Gamma_{11}^1 \mathbf{u}_{,1} \cdot \mathbf{g}_2 = (\mathbf{u}_{,11} - \Gamma_{11}^1 \mathbf{u}_{,1}) \cdot \mathbf{g}_2, \quad \kappa = (u_{\alpha,11} - \Gamma_{11}^1 u_{\alpha,1}) x_{,2}^\alpha. \quad (17)$$

### 3.3. STRAIN AT AN ARBITRARY POINT

If we define position vectors of an arbitrary point in the reference and deformed configurations as:

$$\mathbf{r}(\xi, \eta) = \bar{\mathbf{r}} = \mathbf{r}(\xi) + \eta \mathbf{g}_2, \quad \bar{\mathbf{r}}^*(\xi, \eta) = \bar{\mathbf{r}}^* = \mathbf{r}^*(\xi) + \eta \mathbf{g}_2^*, \quad (18)$$

the base vector at an arbitrary point of a cross section with respect to  $\xi$  coordinate is:

$$\bar{\mathbf{g}}_1 = \mathbf{g}_1 + \eta \mathbf{g}_{2,1}. \quad (19)$$

Using the expression for the first derivative of normal base vector:

$$\frac{d\mathbf{g}_2}{d\xi} = -K \mathbf{g}_1, \quad (20)$$

base vector  $\bar{\mathbf{g}}_1$  with respect to the reference and deformed configurations is:

$$\begin{aligned} \bar{\mathbf{g}}_1 &= \mathbf{g}_1 - \eta K \mathbf{g}_1 = (1 - \eta K) \mathbf{g}_1 = g_0 \mathbf{g}_1, \quad g_0 = 1 - \eta K, \\ \bar{\mathbf{g}}_1^* &= (1 - \eta K^*) \mathbf{g}_1^* \Rightarrow \bar{\mathbf{g}}_1^* = g_0^* \mathbf{g}_1^*, \quad g_0^* = 1 - \eta K^*. \end{aligned} \quad (21)$$

Now, strain at an arbitrary point of a cross section reduces to:

$$\varepsilon_{11}(\eta) = \bar{\varepsilon}_{11} = \frac{1}{2}(\bar{g}_{11}^* - \bar{g}_{11}) = \frac{1}{2}(g_0^{*2} g_{11}^* - g_0^2 g_{11}). \quad (22)$$

which, after insertion of XX and neglecting higher order terms of strain, transforms to:

$$\bar{\varepsilon}_{11} = g_0 [(1 + \eta K) \varepsilon_{11} - \eta \kappa]. \quad (23)$$

This expression is derived rigorously, without any additional geometric assumptions besides the BE hypothesis and the ones regarding finite (but small) strain theory, [5].

### 3.4. FINITE ELEMENT FORMULATION

Stress-strain relation for linear elastic material, at an arbitrary point, is:

$$\bar{\sigma}^{11} = E(\bar{g}^{11})^2 \bar{\varepsilon}_{11}, \quad (24)$$

where  $E$  is the modulus of elasticity, while  $\bar{g}^{11}$  is the determinant of the contravariant metric tensor at an arbitrary point. Now, the internal virtual work can be written as:

$$\delta W_{\text{int}} = \int_V (\bar{g}^{11})^2 \bar{\varepsilon}_{11} E \delta \bar{\varepsilon}_{11} dV. \quad (25)$$

If we recall basic relations:

$$dV = \sqrt{\bar{g}_{11}} d\xi d\eta d\zeta, \quad \sqrt{\bar{g}_{11}} = g_0 \sqrt{g_{11}}, \quad \bar{g}^{11} = \frac{1}{g_0^2} g^{11}, \quad (26)$$

and introduce (23) into (25), the internal component of the virtual work reduces to:

$$\delta W_{\text{int}} = \int_{\xi} (\bar{N} \delta \varepsilon_{11} + \bar{M} \delta \kappa) \sqrt{g_{11}} d\xi, \quad (27)$$

where  $\bar{N}$  and  $\bar{M}$  are section forces energetically conjugated to the reference strains of the beam axis:

$$\bar{N} = \int_A (1 + \eta K) g_0^2 \bar{\sigma}^{11} d\eta d\zeta, \quad \bar{M} = - \int_A \eta g_0^2 \bar{\sigma}^{11} d\eta d\zeta. \quad (28)$$

which differ from the standard section forces. After integration, we obtain:

$$\bar{N} = E(g^{11})^2(A\varepsilon_{11} - \bar{I}\kappa), \quad \bar{M} = E(g^{11})^2(-\bar{I}\varepsilon_{11} + I\kappa), \quad (29)$$

where the appropriate cross section geometric properties are introduced:

$$A = \int_A \frac{(1+\eta K)^2}{g_0} d\eta d\zeta, \quad \bar{I} = \int_A \frac{\eta(1+\eta K)}{g_0} d\eta d\zeta, \quad I = \int_A \frac{\eta^2}{g_0} d\eta d\zeta = \frac{\bar{I}}{2K}. \quad (30)$$

The matrix form of the equation (29) can be written as:

$$\begin{bmatrix} \bar{N} \\ \bar{M} \end{bmatrix} = E(g^{11})^2 \begin{bmatrix} A & -\bar{I} \\ -\bar{I} & I \end{bmatrix} \cdot \begin{bmatrix} \varepsilon_{11} \\ \kappa \end{bmatrix} \Leftrightarrow \bar{\mathbf{R}} = \bar{\mathbf{D}}\boldsymbol{\varepsilon}. \quad (31)$$

For the isogeometric finite element with control points  $I = 1, 2, 3 \dots N$ , the relation between the vector of the reference strains of the beam axis and the vector of displacements of control points is introduced:

$$\boldsymbol{\varepsilon} = \mathbf{B}\mathbf{q}, \quad \boldsymbol{\varepsilon}^T = [\varepsilon_{11} \quad \kappa], \quad (32)$$

where the appropriate vectors and matrices are defined:

$$\mathbf{B} = [\mathbf{B}_1 \quad \mathbf{B}_2 \quad \dots \quad \mathbf{B}_I \quad \dots \quad \mathbf{B}_N], \quad \mathbf{q}^T = [\mathbf{q}_1 \quad \mathbf{q}_2 \quad \dots \quad \mathbf{q}_I \quad \dots \quad \mathbf{q}_N], \quad (33)$$

$$\mathbf{B}_I = \begin{bmatrix} x_{1,1}R_{I,1} & x_{2,1}R_{I,1} \\ x_{1,2}(R_{I,11} - \Gamma_{11}^1 R_{I,1}) & x_{2,2}(R_{I,11} - \Gamma_{11}^1 R_{I,1}) \end{bmatrix}, \quad \mathbf{q}_I = [u_I^1 \quad u_I^2].$$

These designations enable us to represent the internal component of the virtual work as:

$$\delta R_u = \mathbf{q}^T \int_{\xi} \mathbf{B}^T \bar{\mathbf{D}} \mathbf{B} \sqrt{g_{11}} d\xi \delta \mathbf{q}, \quad (34)$$

where:

$$\mathbf{K} = \int_{\xi} \mathbf{B}^T \bar{\mathbf{D}} \mathbf{B} \sqrt{g_{11}} d\xi \quad (35)$$

is the linear stiffness matrix of a rotation-free BE isogeometric finite element, [7].

## 4. NUMERICAL STUDY

Two examples are studied: circular and a free-form cubic beam. Convergence analysis is performed in such a way that the order of convergence is observed as a function of a number of elements  $n_{el}$ , analogously to [10]. Expected values are  $p+1$  for displacements,  $p$  for normal force and  $p-1$  for bending moment, [11]. The order of convergence, for a mesh with  $n_{el}$  elements, is here determined as:

$$\left| \log_{10} \frac{|S_{n_{el}}^h - S^{ex}|}{|S_{n_{el}-1}^h - S^{ex}|} \right| / \log_{10} \left( \frac{n_{el}}{n_{el}-1} \right)$$

where  $S^{ex}$  is the reference solution while  $S_i^h$  is an approximate solution for a mesh with  $i$  elements. Results obtained with very dense meshes are utilized as the reference values, except for the quantities for which these solutions are analytically defined. Since it is noticed that the order of convergence significantly oscillates for some variables and meshes under considerations, these parts graphs are truncated to enable readability.

### 4.1. CIRCULAR ARCH

Fig. 5 shows disposition and properties of a clamped circular arch. Prominent feature of this example is concentrated force at the middle of structure. Due to this load, model does not have  $C^3$  at this section. Therefore, it is interesting to observe the behavior of quartic NURBS using this interelement continuity.

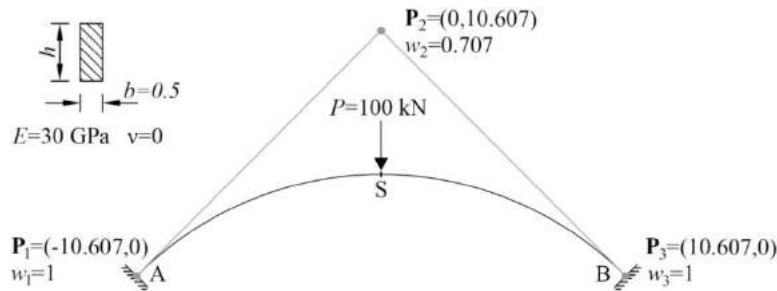


Figure 5. Clamped circular arch under concentrated load.

Convergence properties for  $Kh = 0.067$  are represented in Fig. 6, Fig. 7, Fig. 8, Fig. 9 and Fig. 10. Convergence of deflections is fast, especially for quartics, Fig. 6. Quadratic NURBS returns the order of convergence which is lower than expected value of 3. For cubics, this order converges to predicted value. Regarding quartic NURBS, model with  $C^3$  continuity returns extremely low order of convergence, while solutions for models with lower continuities converge with very high orders.

Regarding convergence of normal force at the section S, it is noticed that all models return expected orders of convergence, Fig. 7. Exception is quartic NURBS with  $C^3$  continuity, which returns lower accuracy. This is due to the coupling of normal force with flexural strain. Notice that similar results are obtained at the support, disregarding the mentioned phenomenon of the highest continuity for quartic elements, Fig. 9.

Generally, convergence properties of bending moments are in line with analytical predictions. Fig. 8 reveals that the orders of convergence for models with quartic NURBS is oscillatory. Again, model with  $C^3$  continuity has very low accuracy. Note that the orders of convergence for both models with cubic NURBS converge to the same value  $p - 1 = 2$ . However, it is evident that model with  $C^2$  continuity has average higher order of convergence, which results with better accuracy per DOF, compared to the  $C^1$  model. At the support, quadratics and cubics behave similarly as at S. Nevertheless, quartics have very high accuracy while their orders of convergence could not be detected, Fig. 10.

Fig. 11 shows excellent correspondence of distribution of bending moments and normal forces along beam. Although not presented, straight BE beam element in Abaqus, B23, requires dense meshes for convergence of section forces.

Fig. 12 displays relative error of considered beam models with respect to 2D isotropic and 2D orthotropic model. 2D models are created using dense meshes of CPS3 elements in Abaqus. Orthotropic material model is made by multiplication of modulus of elasticity along  $\eta$  direction and shear modulus with an empirically determined factor of  $100Kh$ , [10]. This calibrated orthotropic material model is introduced in order to artificially introduce BE assumptions into general 2D model. Result is evident from Fig. 12b, where excellent correspondence of present and calibrated orthotropic 2D model is noticed, even

for high values of curviness  $Kh$ . For more detail discussion on influence of curviness on beam models, see [7] and [10].

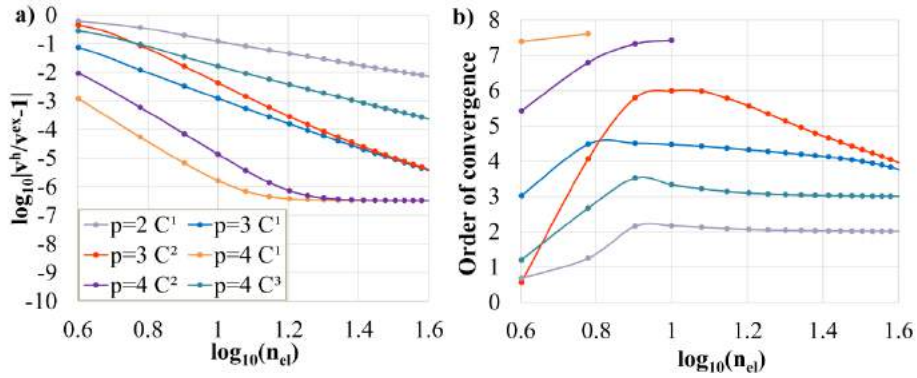


Figure 6. Convergence properties for the deflection at  $S$  using the  $h$ -refinement with different NURBS orders and continuities: a) relative error; b) order of convergence.

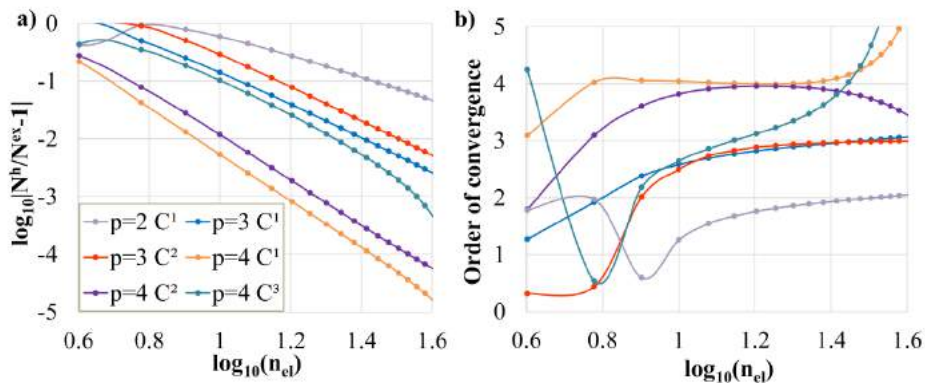


Figure 7. Convergence of the normal force at  $S$  using the  $h$ -refinement with different NURBS orders and continuities: a) relative error; b) order of convergence.

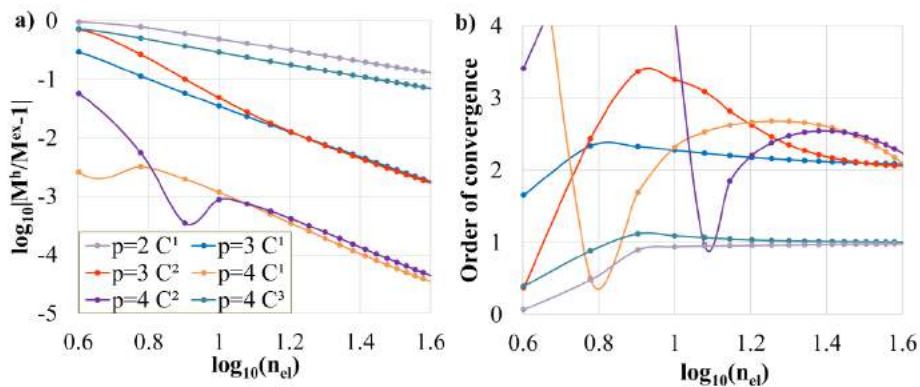


Figure 8. Convergence of the bending moment at  $S$  using the  $h$ -refinement with different NURBS orders and continuities: a) relative error; b) order of convergence.

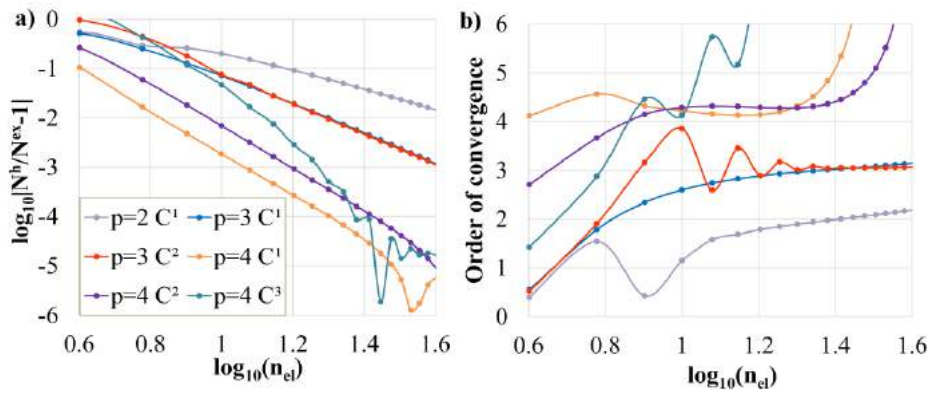


Figure 9. Convergence of the normal force at A using the h-refinement with different NURBS orders and continuities: a) relative error; b) order of convergence.

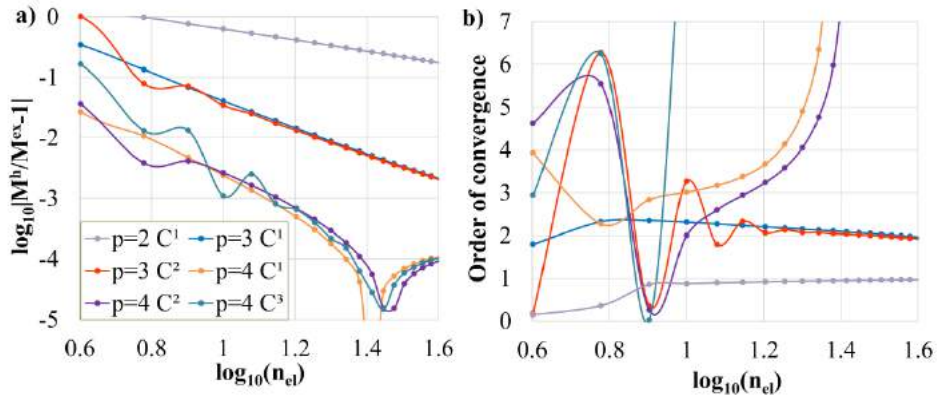


Figure 10. Convergence of the bending moment at A using the h-refinement with different NURBS orders and continuities: a) relative error; b) order of convergence.

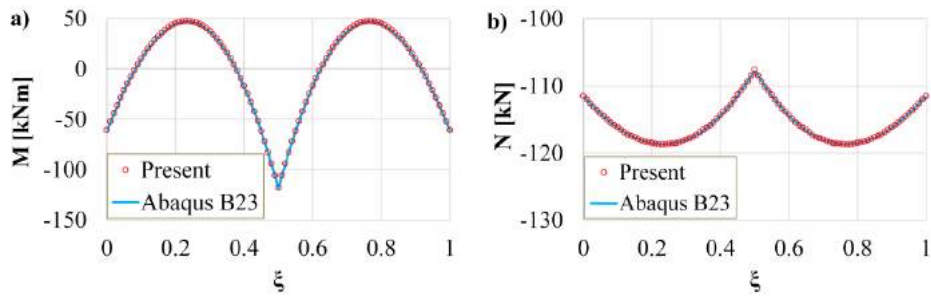


Figure 11. Distribution of: a) bending moment, b) normal force.

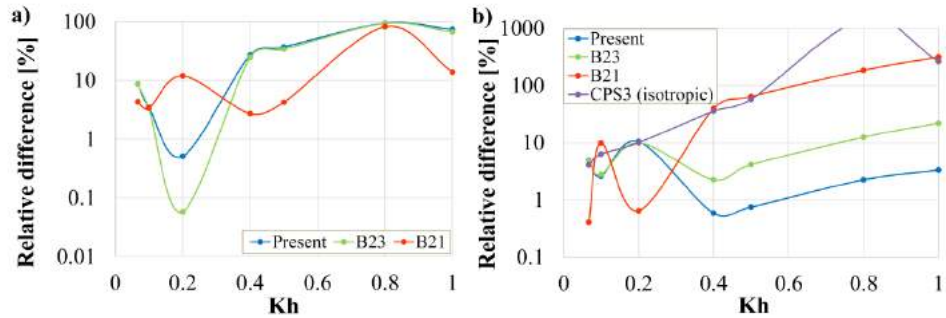


Figure 12. Relative difference of deflection at  $S$ : a) vs. isotropic 2D CPS3 model, b) vs. orthotropic 2D CPS3 model.

#### 4.2. CUBIC ARCH

This example deals with cubic arch presented in Fig. 13. Half of the structure is analyzed using symmetry. This example does not suffer from the problem of discontinuity, as the previous one, since the external load acts at the end point, due to symmetry. However, 2D model is created in Abaqus for comparison and it has well-known issues with pinned support due to stress and strain concentration.

Convergence properties are given in Fig. 14, Fig. 15, Fig. 16, Fig. 17 and Fig. 18. Fig. 14 shows that all models yield very high orders of convergence for deflection, where only those for cubics are well-defined and converge to the expected value of  $p + 1 = 4$ . Results in Fig. 15 suggest that some polynomial degrees return analytical values of the order of convergence for normal force at  $S$  but this is not true for all. Cubics with  $C^1$  have improved accuracy and their orders of convergence could not be determined, as well as those for  $C^3$  quartics and quintics. The same section force at the support has highly oscillatory behavior of the orders of convergence, Fig. 17. Interestingly, cubic and quartic NURBS with highest continuity return orders which are in line with expectations. It is not straightforward to make conclusion regarding relation of accuracy and continuity since for cubics, improved accuracy is evident for model with higher continuity, while it is contrary for quintics.

Convergence of bending moments reveals some expected properties. For the section at  $S$ , all models converge to the predicted value, except for the quintics with  $C^4$  continuity, Fig. 16. Here, improved accuracy of models with highest continuity is evident. Highly oscillatory behavior of the order of convergence for bending moment at the support is observed in Fig. 18b and some parts of graphs had to be truncated. Close inspection suggests that cubic and quartics behave closely to predictions, and improved accuracy per DOF for models with the highest continuity is observed. Quintics return great accuracy while their orders of convergence are not detectable.

In Fig. 19, nearly full compliance of distributions of section forces is obtained via comparison with B23 element from Abaqus. Detail comparison of relative error of beam models with respect to the isotropic model, made of general S3 shell elements in Abaqus, is given in Fig. 20 for different values of curviness. It is evident that present model returns the worst compliance with general shell model. Concretely, present model is the stiffest of all four. This is due to the strictly defined metric of a beam, not present for straight B21 and B23 elements, and BE hypothesis.

Finally, distribution of stresses for two values of curviness is presented in Fig. 21. In Abaqus S3 model, maximum principle stress is displayed. For lower values of curviness, uniaxial stress/strain assumption of BE theory yields good estimate. Still, for extremely large values of curviness, all stress and strain components are significant. Additionally, stress concentration at the pinned support for S3 shell model becomes more prominent as the value of curviness increase. These extreme ranges of stress are marked with gray and black in legend for  $K_{max}h = 1$  and they are hardly visible in given contour plot.

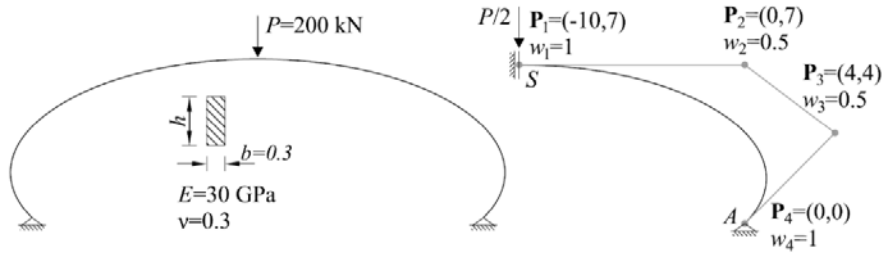


Figure 13. Simply supported free-form cubic arch under concentrated load.

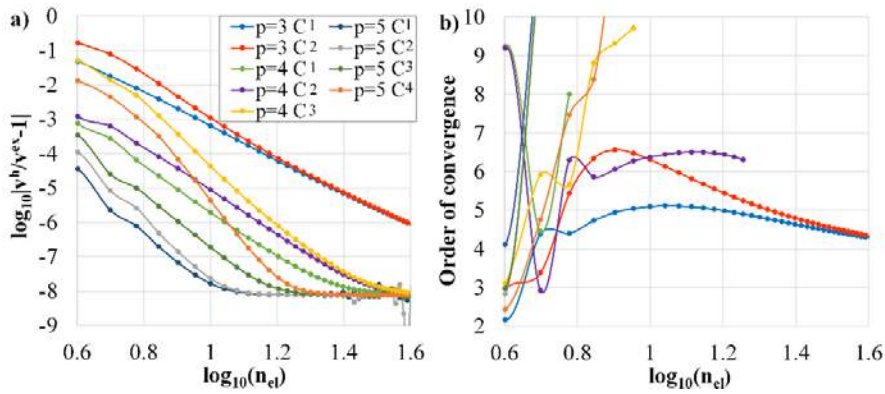


Figure 14. Convergence of the deflection at S using the h-refinement with different NURBS orders and continuities: a) relative error; b) order of convergence.

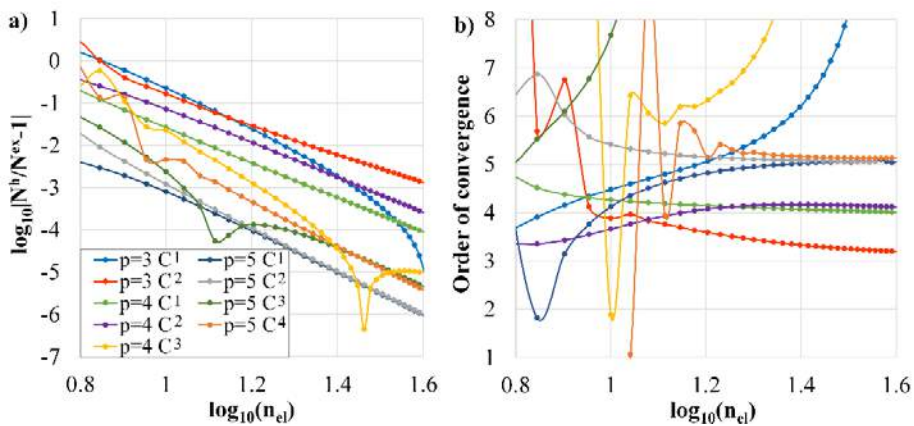


Figure 15. Convergence of the normal force at S using the h-refinement with different NURBS orders and continuities: a) relative error; b) order of convergence.

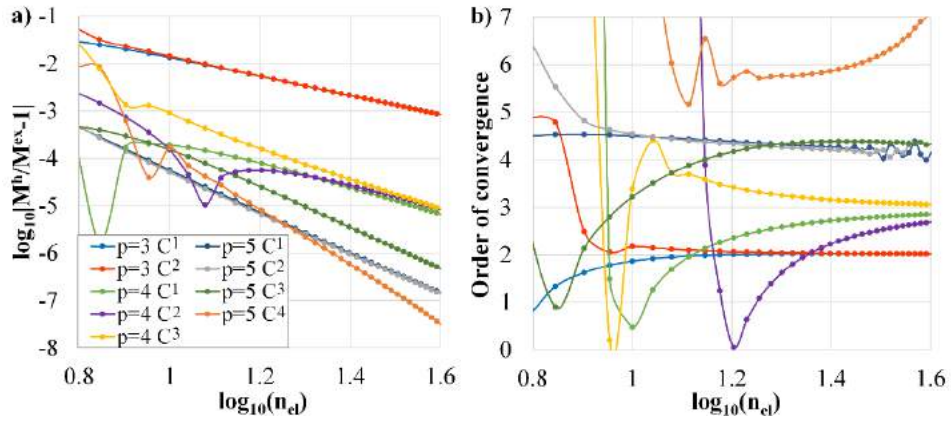


Figure 16. Convergence of the bending moment at S using the h-refinement with different NURBS orders and continuities: a) relative error; b) order of convergence.

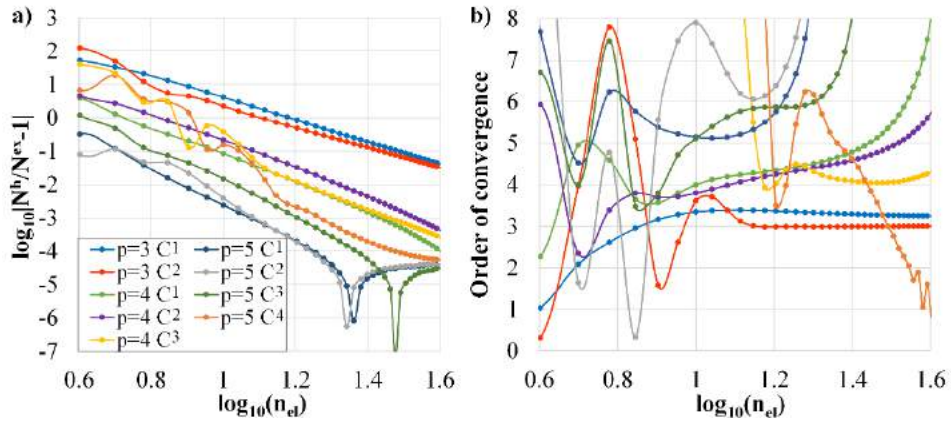


Figure 17. Convergence of the normal force at A using the h-refinement with different NURBS orders and continuities: a) relative error; b) order of convergence.

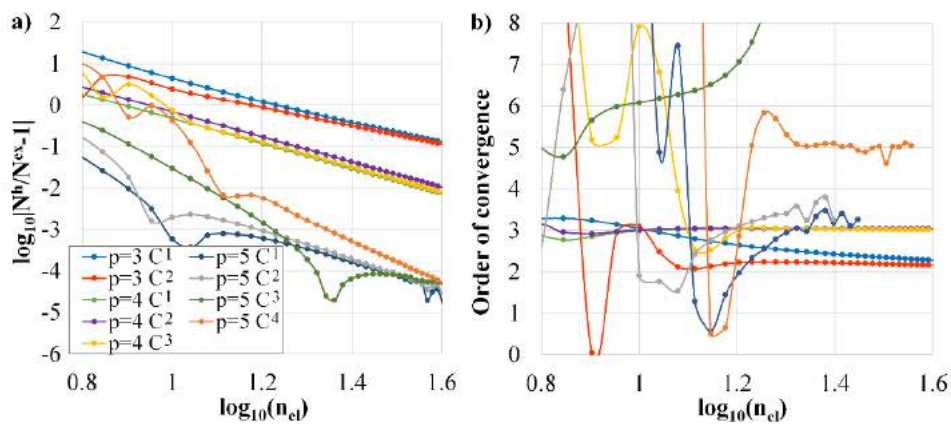


Figure 18. Convergence of the bending moment at A using the  $h$ -refinement with different NURBS orders and continuities: a) relative error; b) order of convergence.

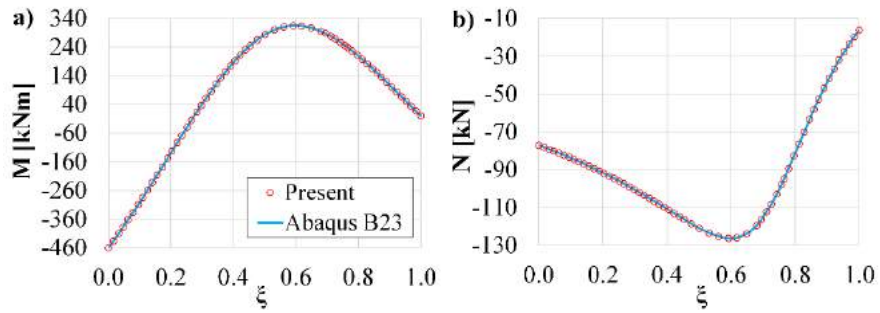


Figure 19. Distribution of: a) bending moment, b) normal force.

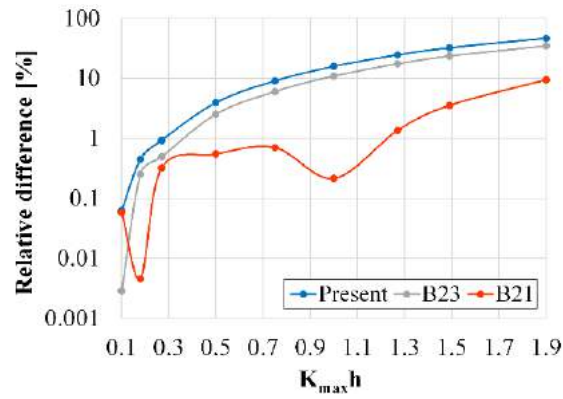


Figure 20. Relative differences of deflections at S with respect to 2D model vs.  $K_{\max} h$ .

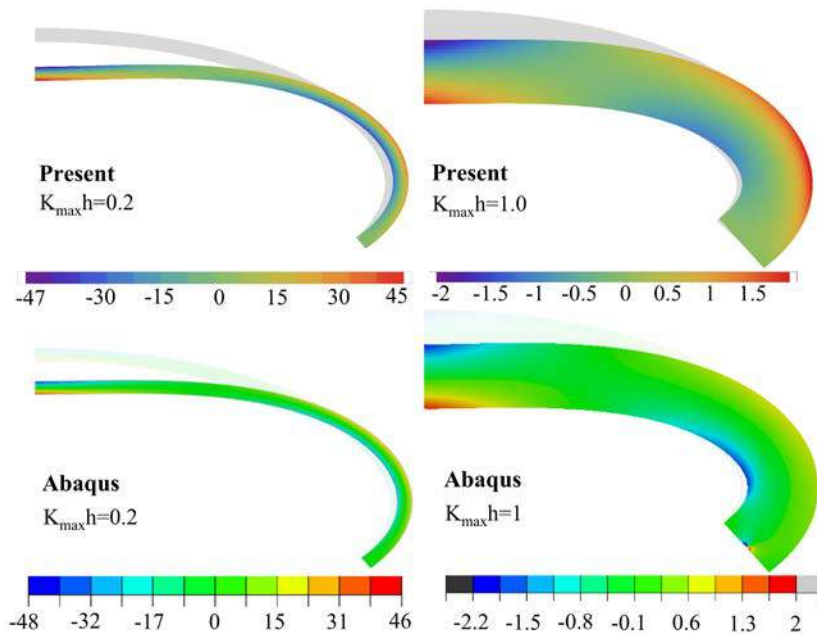


Figure 21. Stress distribution on deformed configuration for two values of curviness

## 5. CONCLUSIONS

Thorough numerical analysis of recently developed computational model of an arbitrarily curved beam is performed via two examples. Due to rigorously defined metric and BE assumptions, present model is stiffer than standard beam models. It is concluded that the order of convergence is improved for the most meshes with highest continuity. However, for models that have interelement discontinuity of some order, increase in continuity must be considered carefully, since it could result with reduced accuracy.

Further research will be focused on a finite rotation and finite strain dynamic analysis of plane and spatial beams.

## LITERATURE

- [1] T. Hughes, J. Cottrell and Y. Bazilevs, "Isogeometric analysis: CAD, finite elements, NURBS, exact geometry and mesh refinement," *Comput. Methods Appl. Mech. Engrg.*, vol. 194, pp. 4135-4195, 2005.
- [2] T. Hughes, *The Finite Element Method: Linear Static and Dynamic Finite Element Analysis*, New Jersey: Prentice-Hall, 1987.
- [3] T. Hughes, "Isogeometric analysis: Progress and challenges," *Comput. Methods Appl. Mech. Engrg.*, vol. 316, p. 1, 2017.
- [4] A. Cazzani, M. Malagu, E. Turco and F. Stochino, "Constitutive models for strongly curved beams in the frame of isogeometric analysis," *Mathematics and Mechanics of Solids*, vol. 21, no. 2, pp. 189-209, 2016.

- [5] G. Radenković, *Isogeometric theory of structures* (in Serbian), Belgrade: Faculty of Architecture, 2014.
- [6] G. Radenković, *Finite rotation and finite strain isogeometric structural analysis* (in Serbian), Beograd: Faculty of Architecture, 2017.
- [7] A. Borković, S. Kovačević, G. Radenković, S. Milovanović and M. Guzijan-Dilber, "Rotation-free isogeometric analysis of an arbitrarily curved plane Bernoulli-Euler beam," *Comput. Methods Appl. Mech. Engrg.*, vol. 334, pp. 238-267, 2018.
- [8] J. Cottrell, T. Hughes and Y. Bazilevs, *Isogeometric analysis: Toward integration of CAD and FEA*, Chichester: Wiley, 2009.
- [9] L. Piegl and W. Tiller, *The NURBS Book*, Springer, 1995.
- [10] A. Borković, S. Kovačević, G. Radenković, S. Milovanović and D. Majstorović, "Rotation-free isogeometric analysis of in-plane free vibrations of an arbitrarily curved Bernoulli-Euler beam," *submitted to Engineering structures*.
- [11] Y. Bazilevs, L. Beirao da Veiga, J. Cottrell, T. J. R. Hughes and G. Sangalli, "Isogeometric analysis: approximation, stability and error estimates for h-refined meshes," *Mathematical Models and Methods in Applied Sciences*, vol. 16, no. 7, pp. 1031-1090, 2006.